Journal of Photochemistry and Photobiology A: Chemistry 202 (2009) 10–20

Contents lists available at ScienceDirect

Journal of Photochemistry and Photobiology A: Chemistry

journal homepage: www.elsevier.com/locate/jphotochem

Spectroscopic properties of lanthanoid benzene carboxylates in the solid state: Part 1

Matthias Hilder[a], Peter C. Junk[a,*], Ulrich H. Kynast[b], Marina M. Lezhnina[b]

[a] School of Chemistry, Monash University, Clayton, Vic. 3800, Australia
[b] University of Applied Sciences Muenster, Department of Chemical Engineering/Applied Materials Sciences, Stegerwaldstr. 39, 48 565 Steinfurt, Germany

ARTICLE INFO

Article history:
Received 9 June 2008
Received in revised form 29 October 2008
Accepted 31 October 2008
Available online 19 November 2008

Keywords:
Lanthanoids
Carboxylates
Benzoates
Luminescence
Solid state

ABSTRACT

Europium and terbium complexes of benzoic acid (HBA), 9-anthracene carboxylic acid (9-HACA), 1-naphthoic acid (1-HNA), 2-naphthoic acid (2-HNA), cinnamic acid (HCA), *o*-phenylbenzoic acid (*o*-HPhBA), *p*-phenylbenzoic acid (*p*-HPhBA), *o*-methylbenzoic acid (*o*-HMeBA), *m*-methylbenzoic acid (*m*-HMeBA), *p*-methylbenzoic acid (*p*-HMeBA), *p*-*tert*-butylbenzoic acid (*p*-^{tert}HBuBA), phthalic acid (H_2Phth), isophthalic acid (H_2-IsoPhth) and terephthalic acid (H_2-TerePhth) were synthesised by aqueous metathesis reactions. The compositions were determined by microanalysis, DTA, and EDTA volumetric methods. Structural conclusions were drawn from powder XRD patterns and IR spectra. The optoelectronic properties were determined in the solid state, including reflectance, excitation, emission, and excitation efficiency, complemented by considering triplet state energies, which were derived from phosphorescence spectra of the corresponding gadolinium complexes. Besides the emission efficiencies, the splitting pattern of the $^5D_0 \rightarrow {}^7F_J$ transitions of Eu^{3+} were used to derive structural information and the intensities relative to the $^5D_0 \rightarrow {}^7F_J$ were used to gain information about the mechanism, adding electronic allowed dipole character to the forbidden emissions.

1. Introduction

Lanthanoid complexes represent popular luminescent materials used for various optical applications, including biological fluoro-immuno assays [1], lasers [2], lighting systems [3], electroluminescent devices and diodes [4,5], cathode ray tubes [6], sensors [7], dosimeters [8], imaging agents [9], display applications [10] and decoration purposes [11]. The popularity of lanthanoids in optical devices is related to their unique photophysical properties. Lanthanoids are line emitters and furthermore their emission lines are considered invariable and therefore almost independent of crystal field effects, resulting in very pure emission colours. These properties are a consequence of the shielding effect, due to the outer 5*s* and 5*p* electrons shielding the inner 4*f* valence electrons from interactions with the surrounding crystal field, resulting (even in the solid state) in lanthanoids being electronically treated as isolated centres [12–19]. Therefore, the predominant property the individual lanthanoid contributes to the coordination chemistry is its radius [7,20,21].

In spite of all these advantages, however, there are some disadvantages. Lanthanoids cannot be excited directly. Due to their quantum mechanically forbidden character, the molar absorption coefficient α for $f \rightarrow f$ transitions is low (10^{-3} to 10 $dm^3/cm\,mol$), meaning they cannot be effectively excited by electromagnetic radiation [12,15,16,19,22,23].

However, it has been observed that the excitation of strongly absorbing organic ligands coordinated to the lanthanoid centre enhances lanthanoid luminescence immensely. The organic chromophore absorbs light due to a singlet → singlet absorption. From the excited singlet state the ligand relaxes non-radiatively to its triplet state. Spin forbidden intersystem crossing is induced by spin-orbit coupling (enhanced through the presence of heavy lanthanoid ions). Under certain circumstances the energy of the triplet state is transferred to the excited lanthanoid state by a Coulomb energy transfer mechanism. From the excited lanthanoid state the system relaxes into the lanthanoid ground state. The radiative relaxation is accompanied by the emission of very characteristic lanthanoid emission lines. Since the organic chromophore acts as a photon collector, which excites the lanthanoid indirectly, the phenomenon can be described as ligand sensitised luminescence. This process is also known as the antenna effect [9,22,24]. In contrast to the lanthanoid ions, these complexes exhibit large Stokes shifts, thus they have been also referred to as light converting molecular devices (LCMDs) [25].

Many different ligand classes have been studied (including β-diketonates [26], carboxylates [27,28], macrocyclic ether complexes [29] or complexes co-coordinated by bulky co-ligands such as bipyridine, phenanthroline or terpyridine [4,5] and their single

* Corresponding author. Tel.: +61 3 9905 4570; fax: +61 3 9905 4597.
E-mail address: peter.junk@sci.monash.edu.au (P.C. Junk).

1010-6030/$ – see front matter © 2008 Elsevier B.V. All rights reserved.
doi:10.1016/j.jphotochem.2008.10.026

Table 1
Ligands used in this work.

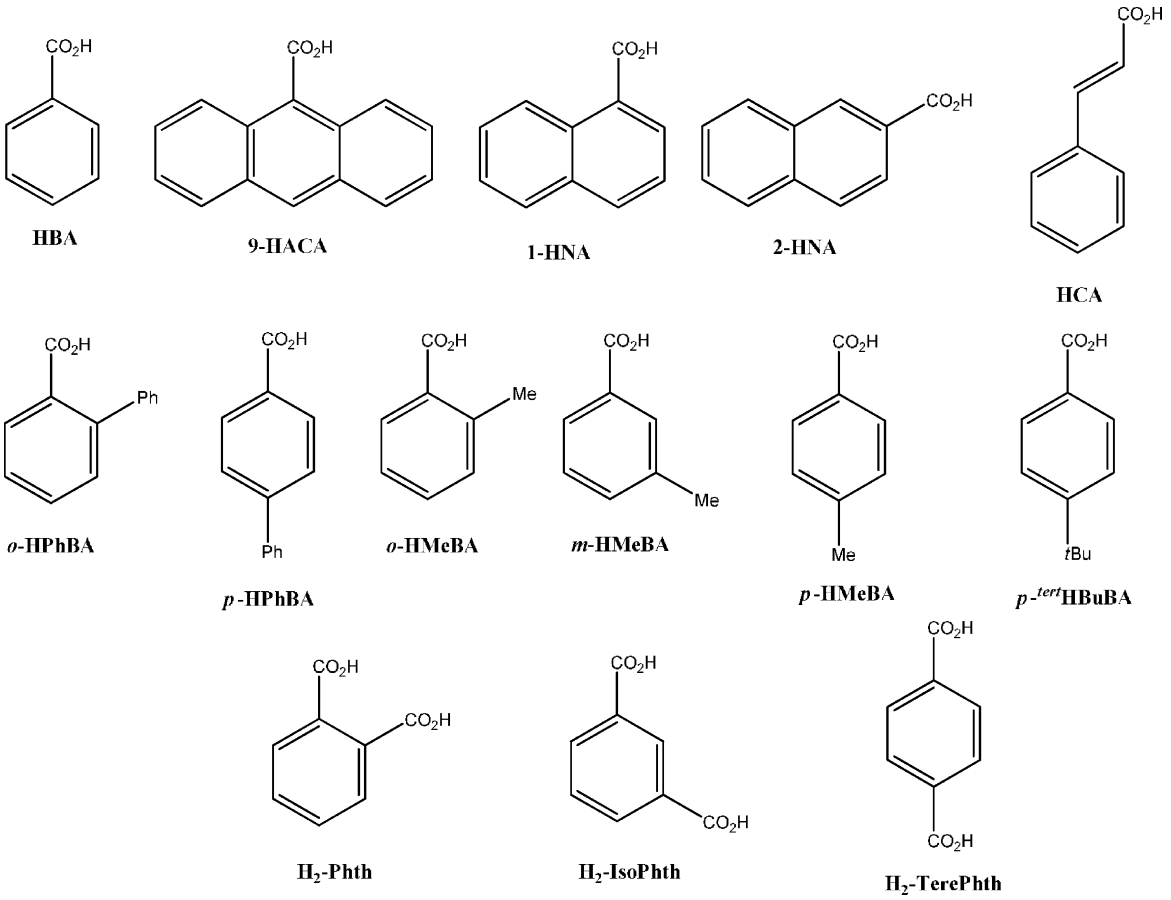

crystal X-ray structures determined [30]. These have been characterised in various forms, in the solid state, in solution, or doped into different host matrices for example polymers [31], sol–gels [32], glasses [33], lyotropic mesophases [34] and zeolites [27,35,36].

For this study, europium, terbium and gadolinium complexes of benzoic acid derivatives have been synthesised. In contrast to europium and terbium complexes, whose luminescence can be sensitised by coordinated ligands (Eu^{3+}: red $^5D_0 \rightarrow {}^7F_1$ emission; Tb^{3+}: green the $^5D_0 \rightarrow {}^7F_5$ emission), Gd compounds do not emit visible light. However, the phosphorescence spectra of those complexes show signals resulting from triplet → singlet transitions and are thus reflecting the triplet state energies of the coordinated ligands. The benzoate ligands were chosen since the carboxylate group interacts strongly with the oxophilic lanthanoids and the delocalised π electron system provides a strongly absorbing chromophore.

Despite the enormous number of publications regarding the emission properties of lanthanoid benzoate derivatives the results are not always easy to compare quantitatively [37,38]. The results are very sensitive to the chosen characterisation conditions such as temperature, concentration, solvent, excitation wavelength and data processing to name a few.

The aim of this study was to determine the photophysical properties of europium and terbium compounds, coordinated to aromatic carboxylate derivatives, systematically functionalised by hydrocarbon substituents in their neatest and most simple form, namely, in the solid state as they precipitate from aqueous reaction mixtures. The photophysical properties were determined using invariable instrument parameters, measuring conditions and correction procedures. This comprehensive and systematic study shows correlations between the composition of the complexes, the nature, degree and position of substitution, the lanthanoid centre and the emission efficiency.

2. Results and discussion

2.1. Synthesis

All europium and terbium carboxylate complexes were synthesised by aqueous metathesis reactions (Eq. (1)). The carboxylic acid was converted into the sodium salt by addition of sodium bicarbonate to the aqueous ligand suspension until a clear solution was formed and a pH of five was reached. To this, standardised europium or terbium chloride solutions were added (Ln:acid ratio = 1:3; 2:3 for diprotic ligands) at room temperature, resulting in the formation of insoluble precipitates of the corresponding lanthanoid carboxylates. Following this synthetic route, europium and terbium complexes of benzoic acid (HBA), 9-anthracene carboxylic acid (9-HACA), 1-naphthoic acid (1-HNA), 2-naphthoic acid (2-HNA), cinnamic acid (HCA), *o*-phenylbenzoic acid (*o*-HPhBA), *p*-phenylbenzoic acid (*p*-HPhBA), *o*-methylbenzoic acid (*o*-HMeBA), *m*-methylbenzoic acid (*m*-HMeBA), *p*-methylbenzoic acid (*p*-HMeBA), *p*-^{tert}butylbenzoic acid (*p*-^{tert}HBuBA), phthalic acid (H_2Phth), isophthalic acid (H_2-IsoPhth) and terephthalic acid (H_2-TerePhth) (see Table 1) were synthesised. The isolated yields ranged from 35 to 94% but were generally in the vicinity of 70%. The gadolinium complexes were synthesised in an identical manner.

$$LnCl_{3(aq)} + 3NaL_{(aq)} \rightarrow 3NaCl_{(aq)} + LnL_{3(s)} \quad (1)$$

Table 2
Microanalytical data for all complexes.

Composition	Europium		Composition	Terbium	
	Determined	Calculated		Determined	Calculated
$Eu(BA)_3(H_2O)$	NA* C = 47.5%	NA* C = 47.3%	$Tb(BA)_3(H_2O)_4$	Gd = 26.7% C = 42.2%	Gd = 26.7% C = 42.4%
$Eu(1\text{-}NA)_3(H_2O)$	Eu = 22.3% C = 57.5%	Eu = 22.2% C = 58.0%	$Tb(1\text{-}NA)_3(H_2O)$	Gd = 23.1% C = 57.6%	Gd = 23.0% C = 57.4%
$Eu(2\text{-}NA)_3(H_2O)_2$	Eu = 21.4% C = 55.8%	Eu = 21.6% C = 56.5%	$Tb(2\text{-}NA)_3(H_2O)_2$	Gd = 22.0% C = 56.8%	Gd = 22.4% C = 55.9%
$Eu(o\text{-}PhBA)_3(H_2O)_2$	Eu = 19.5% C = 58.9%	Eu = 19.5% C = 60.1%	$Tb(o\text{-}PhBA)_3(H_2O)_2$	Gd = 20.3% C = 60.4%	Gd = 20.2% C = 59.6%
$Eu(p\text{-}PhBA)_3(H_2O)_2$	Eu = 19.5% C = 59.3%	Eu = 19.5% C = 60.1%	$Tb(p\text{-}PhBA)_3(H_2O)_4$	Gd = 20.3% C = 58.7%	Gd = 20.2% C = 59.6%
$Eu(CA)_3$	Eu = 26.0% C = 55.1%	Eu = 25.6% C = 54.6%	$Tb(CA)_3$	Gd = 26.3% C = 54.5%	Gd = 26.5% C = 54.0%
$Eu(9\text{-}ACA)_3$	Eu = 18.3% C = 66.1%	Eu = 1 8.6% C = 66.3%	$Tb(9\text{-}ACA)_3$	Gd = 19.7% C = 65.9%	Gd = 19.3% C = 65.7%
$Eu(p\text{-}^{tert.}BuBA)_3$	Eu = 22.2% C = 57.0%	Eu = 22.2% C = 58.0%	$Tb(p\text{-}^{tert.}BuBA)_3$	Gd = 23.0% C = 56.6%	Gd = 23.0% C = 57.4%
$Eu(o\text{-}MeBA)_3(H_2O)$	Eu = 26.2% C = 50.9%	Eu = 26.4% C = 50.1%	$Tb(o\text{-}MeBA)_3(H_2O)$	Gd = 27.1% C = 50.6%	Gd = 27.3% C = 49.5%
$Eu(m\text{-}MeBA)_3$	Eu = 27.1% C = 51.8%	Eu = 27.3% C = 51.7%	$Tb(m\text{-}MeBA)_3$	Gd = 28.2% C = 51.9%	Gd = 28.2% C = 51.1%
$Eu(p\text{-}MeBA)_3$	Eu = 27.2% C = 53.2%	Eu = 27.3% C = 51.4%	$Tb(p\text{-}MeBA)_3$	Gd = 28.1% C = 50.4%	Gd = 28.2% C = 51.1%
$Eu_2(Phth)_3(H_2O)_2$	Eu = 36.1% C = 34.5%	Eu = 36.5% C = 34.6%	$Tb_2(Phth)_3(H_2O)_2$	Gd = 36.9% C = 33.2%	Gd = 37.6% C = 34.1%
$Eu_2(IsoPhth)_3(H_2O)_2$	Eu = 37.1% C = 33.1%	Eu = 36.5% C = 34.6%	$Tb_2(IsoPhth)_3(H_2O)_2$	Gd = 38.5% C = 33.9%	Gd = 37.6% C = 34.1%
$Eu_2(TerePhth)_3(H_2O)_4$	Eu = 35.5% C = 34.0%	Eu = 35.0% C = 34.2%	$Tb_2(TerePhth)_3(H_2O)_4$	Gd = 37.2% NA*	Gd = 36.0% NA*

* Not determined due to insufficient amount of compound.

2.2. Composition

The compositions shown in Table 2 are based on microanalysis results (carbon content) and EDTA complexiometry (lanthanoid content).

2.3. Thermogravimetric analysis

Selected complexes were determined by TG/DTA thermoanalytical methods (see Table 3). The results are in agreement with the compositions suggested by microanalytical and complexiometric results (Table 2).

2.4. IR data

The infrared spectra of the complexes have also been recorded. Table 4 shows the assignments of the C=O stretching vibrations of the free ligands, ν(C=O), the symmetric and asymmetric stretching frequencies of the complexes, $\nu_{as}(CO_2^-)$ and $\nu_s(CO_2^-)$, as well as the separation of these two vibrations, $\Delta\nu(CO_2^-)$. Previous studies have suggested that the energy difference of the symmetric and asymmetric bands $\Delta\nu(CO_2^-)$ reflects bonding properties and structural features [39,40]. Carboxylates can be divided into three groups. To the first group belong complexes whose spectra show large $\Delta\nu$ values being larger than 200 cm^{-1}, reflecting carboxylate groups with C_s symmetry (1-naphthoate complexes). The second group of complexes shows a moderate separation of the two carboxylate vibrations, e.g., having $\Delta\nu(CO_2^-)$ values of around 150 cm^{-1} and is observed for complexes which have very symmetric carboxylate groups with C_{2v} symmetry (9-anthracenecarboxylate). Most carboxylates such as the Eu and Tb complexes of benzoic acid, cinnamic acid, 2-naphthoic acid, *p*-phenylbenzoic acid, *p*-^{tert}butylbenzoic acid, methylbenzoic acid (*o*- and *p*-), belong to the third group, showing rather small $\Delta\nu$ values indicating distorted carboxylate groups. The remaining complexes have $\Delta\nu$ values lying between the second and third group (e.g., 135–145 cm^{-1}). All these conclusions are considered to be rough guidelines only since lanthanoid carboxylates usually show more than one type of coordination.

2.5. Phase and structural analysis

X-ray powder diffraction methods were used to determine the phases of the synthesised complexes. Comparing the diffractograms it is evident that most europium and terbium complexes incorporating the same ligand are isostructural. Exceptions are complexes of benzoic acid, *m*-methylbenzoic acid and *p*-methylbenzoic acid.

Some lanthanoid carboxylate crystal structures, incorporating ligands used within this study, had previously been published. Based on this data, X-ray diffractograms were calculated and compared to the measured patterns from this work.

The diffractograms obtained for the europium and terbium benzoate complexes are different from each other, and furthermore, do not match the calculated patterns of the published $\{[Dy(BA)_3(H_2O)_4]H_2O\}_n$ complex [41], meaning there are at least three different structural modifications for benzoates within the lanthanoid series. The same situation applies to the *p*-methylbenzoate complexes. Although it is not surprising that the

Table 3
Weight loss determined by DTA.

Complex	Low temperature weight loss	Equivalent to n number of water molecules	Total weight loss	Expected for oxide formation
$Tb(BA)_3(H_2O)_4$	9% (exo: 105 °C)	9% ($n=3$)	68% (endo: 620 °C)	69%
$Eu(2\text{-}NA)_3(H_2O)_2$	5% (exo: 165 °C)	5% ($n=2$)	75% (endo: 600 °C)	75%
$Tb(o\text{-}PhBA)_3(H_2O)_2$	5% (exo: 120 °C)	5% ($n=2$)	76% (endo: 650 °C)	76%
$Eu(p\text{-}PhBA)_3(H_2O)_2$	5% (exo: 130 + 155 °C)	5% ($n=2$)	78% (endo: 650 °C)	77%
$Eu(o\text{-}MeBA)_3(H_2O)$	3% (exo: 155 °C)	3% ($n=1$)	70% (endo: 700 °C)	69%
$Tb_2(Phth)_3(H_2O)_2$	5% (exo: 210 °C)	4% ($n=2$)	56% (endo: 665 °C)	58%
$Eu_2(IsoPhth)_3(H_2O)_2$	5% (exo: 125 °C)	4% ($n=2$)	56% (endo: 660 °C)	56%

Table 4
Stretching frequencies of C=O and CO_2^- vibrations in cm^{-1}.

Composition	HL	Eu	Tb
$Ln(BA)_3(H_2O)_4$	ν(C=O): 1674		$\nu_{asy}(CO_2^-)$: 1525 $\nu_{sy}(CO_2^-)$: 1410 $\Delta\nu(CO_2^-)$: 115
$Ln(BA)_3(H_2O)$	ν(C=O): 1675	$\nu_{asy}(CO_2^-)$: 1519 $\nu_{sy}(CO_2^-)$: 1399 $\Delta\nu(CO_2^-)$: 120	
$Ln(1\text{-}NA)_3(H_2O)$	ν(C=O): 1666	$\nu_{asy}(CO_2^-)$: 1508 $\nu_{sy}(CO_2^-)$: 1337 $\Delta\nu(CO_2^-)$: 168	$\nu_{asy}(CO_2^-)$: 1518 $\nu_{sy}(CO_2^-)$: 1363–1352 $\Delta\nu(CO_2^-)$: 155–166
$Ln(2\text{-}NA)_3(H_2O)_2$	ν(C=O): 1678	$\nu_{asy}(CO_2^-)$: 1527 $\nu_{sy}(CO_2^-)$: 1419 $\Delta\nu(CO_2^-)$: 108	$\nu_{asy}(CO_2^-)$: 1527 $\nu_{sy}(CO_2^-)$: 1405 $\Delta\nu(CO_2^-)$: 123
$Ln(o\text{-}PhBA)_3(H_2O)_2$	ν(C=O): 1679	$\nu_{asy}(CO_2^-)$: 1530 $\nu_{sy}(CO_2^-)$: 1389 $\Delta\nu(CO_2^-)$: 141	$\nu_{asy}(CO_2^-)$: 1526 $\nu_{sy}(CO_2^-)$: 1395 $\Delta\nu(CO_2^-)$: 131
$Ln(p\text{-}PhBA)_3(H_2O)_2$	ν(C=O): 1672	$\nu_{asy}(CO_2^-)$: 1531 $\nu_{sy}(CO_2^-)$: 1425 $\Delta\nu(CO_2^-)$: 106	$\nu_{asy}(CO_2^-)$: 1520 $\nu_{sy}(CO_2^-)$: 1418 $\Delta\nu(CO_2^-)$: 102
$Ln(CA)_3$	ν(C=O): 1668	$\nu_{asy}(CO_2^-)$: 1490 $\nu_{sy}(CO_2^-)$: 1386 $\Delta\nu(CO_2^-)$: 104	$\nu_{asy}(CO_2^-)$: 1491 $\nu_{sy}(CO_2^-)$: 1377 $\Delta\nu(CO_2^-)$: 114
$Ln(9\text{-}ACA)_3$	ν(C=O): 1672	$\nu_{asy}(CO_2^-)$: 1522 $\nu_{sy}(CO_2^-)$: 1374 $\Delta\nu(CO_2^-)$: 148	$\nu_{asy}(CO_2^-)$: 1524 $\nu_{sy}(CO_2^-)$: 1373 $\Delta\nu(CO_2^-)$: 151
$Ln(p\text{-}^{tert}BuBA)_3$	ν(C=O): 1674	$\nu_{asy}(CO_2^-)$: 1502 $\nu_{sy}(CO_2^-)$: 1380 $\Delta\nu(CO_2^-)$: 122	$\nu_{asy}(CO_2^-)$: 1503 $\nu_{sy}(CO_2^-)$: 1385 $\Delta\nu(CO_2^-)$: 118
$Ln(o\text{-}MeBA)_3(H_2O)$	ν(C=O): 1669	$\nu_{asy}(CO_2^-)$: 1481, 1502 $\nu_{sy}(CO_2^-)$: 1405, 1430 $\Delta\nu(CO_2^-)$: 51, 97	$\nu_{asy}(CO_2^-)$: 1482, 1502 $\nu_{sy}(CO_2^-)$: 1405, 1415 $\Delta\nu(CO_2^-)$: 67, 97
$Ln(m\text{-}MeBA)_3$	ν(C=O): 1675	$\nu_{asy}(CO_2^-)$: 1519 $\nu_{sy}(CO_2^-)$: 1370 $\Delta\nu(CO_2^-)$: 149	$\nu_{asy}(CO_2^-)$: 1518 $\nu_{sy}(CO_2^-)$: 1387 $\Delta\nu(CO_2^-)$: 131
$Ln(p\text{-}MeBA)_3$	ν(C=O): 1664	$\nu_{asy}(CO_2^-)$: 1529 $\nu_{sy}(CO_2^-)$: 1395 $\Delta\nu(CO_2^-)$: 134	$\nu_{asy}(CO_2^-)$: 1518 $\nu_{sy}(CO_2^-)$: 1406 $\Delta\nu(CO_2^-)$: 112
$Ln_2(Phth)_3(H_2O)_2$	ν(C=O): 1657	$\nu_{asy}(CO_2^-)$: 1544, 1512 $\nu_{sy}(CO_2^-)$: 1402 $\Delta\nu(CO_2^-)$: 110, 142	$\nu_{asy}(CO_2^-)$: 1544, 1513 $\nu_{sy}(CO_2^-)$: 1409 $\Delta\nu(CO_2^-)$: 104, 135
$Ln_2(IsoPhth)_3(H_2O)_2$	ν(C=O): 1675	$\nu_{asy}(CO_2^-)$: 1544–1514 $\nu_{sy}(CO_2^-)$: 1393 $\Delta\nu(CO_2^-)$: 121–151	$\nu_{asy}(CO_2^-)$: 1523 $\nu_{sy}(CO_2^-)$: 1396 $\Delta\nu(CO_2^-)$: 137
$Ln_2(TerePhth)_3(H_2O)_4$	ν(C=O): 1664	$\nu_{asy}(CO_2^-)$: 1534 $\nu_{sy}(CO_2^-)$: 1394 $\Delta\nu(CO_2^-)$: 140	$\nu_{asy}(CO_2^-)$: 1536 $\nu_{sy}(CO_2^-)$: 1397 $\Delta\nu(CO_2^-)$: 139

terbium and europium complexes are not isostructural, it is surprising that the europium *p*-methylbenzoate diffraction pattern does not match the calculated diffractogram based on the data of the published $[Eu(p\text{-}MeBA)_3]_n$ structure [42]. This means that there are at least three structural modifications of this ligand within the lanthanoid series and that Eu *p*-methylbenzoate exists in at least two different structural modifications.

The measured diffractograms suggest that europium and terbium *m*-methylbenzoates are not isostructural. However, comparing these to the calculated patterns based on published single crystal data suggests that the europium complex is isostructural with $[Nd(m\text{-}MeBA)_3]_n$ [43], whereas the structure of the terbium complex is identical to the structure of a previously reported terbium complex $[Tb(m\text{-}MeBA)_3]_n$ [43]. Therefore, there are at least two structural modifications of this ligand within the lanthanoid series, with the structural change occurring at either europium or gadolinium.

The structures of europium and terbium phthalate are identical, and furthermore, match the patterns of the published single crystal structures of $\{[Eu_2(Phth)_3(H_2O)](H_2O)\}_n$ [44] and $\{[Tb_2(Phth)_3(H_2O)](H_2O)\}_n$ [44]. Similarly, both synthesised terephthalate complexes are isostructural to $\{[Tb_2(TerePhth)_3(H_2O)](H_2O)\}_n$ [45]. The same applies to the cinnamate complexes regarding the published structure of $[La(CA)_3]_n$ [46].

2.6. Absorption, excitation and emission properties

The optical absorption and emission properties of the complexes have been determined in the solid state (see Section 4 for details and Fig. 1 for a typical excitation and emission spectra, in this case for $Ln(p\text{-}MeBA)_3$] (Ln = Tb, Eu) and are displayed in Table 5. The triplet state energies, determined from room temperature phosphorescence measurements from the corresponding Gd complexes, are presented in Table 6 (the Gd complexes had only been synthesised for comparison purposes and their composition had been characterised by IR spectroscopy). To keep the results comparable, the triplet state energies were determined in the solid state at room temperature. However, some complexes gave only weak signals and thus the measurements were repeated at low temperature (110 K).

In order to transfer the energy from the ligand to the lanthanoid, the triplet state energy needs to be higher than the lanthanoid resonance level (Eu^{3+}: $^5D_0$ state at 17,200 cm^{-1}; Tb^{3+}: $^5D_4$ state at 20,500 cm^{-1}) [7,9,23,47]. Theoretically, the energy difference should be at least 207 cm^{-1} to prevent thermal assisted lanthanoid-ligand energy-back transfer (e.g., thermal energy = kT) [7] but it had been shown that a difference of 2000–2500 cm^{-1} is necessary to sensitise lanthanoid emission efficiently [48].

Comparing the measured triplet energies, the energy differences decreases with increasing degree of conjugation in the order: BA > *o*-PhBA > *p*-PhBA ≈ CA > 2-NA > 1-NA. While the high energetic benzoate triplet state transfers its energy efficiently to the resonance levels of both Eu^{3+} and Tb^{3+}, an increase in conjugation lowers the triplet state energy to such an extent that there is inefficient energy transfer from the triplet state to the lanthanoid

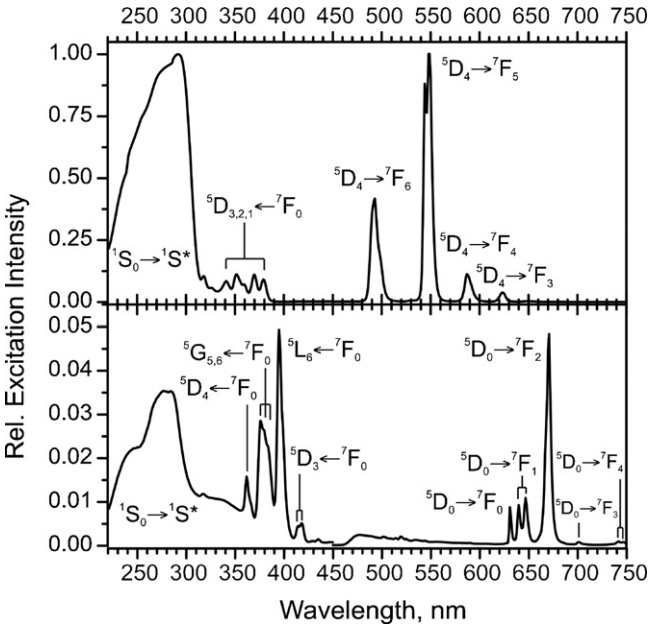

Fig. 1. Solid state excitation and emission spectra of anhydrous Tb(*p*-methylbenzoate)$_3$ (top) and Eu(*p*-methylbenzoate)$_3$ (bottom). $^1S_0 \rightarrow {}^1S^*$ denotes ligand transitions. Note the dramatic intensity difference between the terbium and the europium complex and the unusually pronounced $^5D_0 \rightarrow {}^7F_0$ emission.

resonance level. Consequently, the emission integrals for europium and terbium emission decrease. The triplet state energies for the cinnamate and *p*-phenylbenzoate complexes are similar to the $^5D_4$ level of Tb^{3+}. These ligands only sensitise europium luminescence, populating the lower energetic europium $^5D_0$ state while in the terbium complexes thermally assisted energy-back transfer to the triplet state of the ligand dominates. The conjugation found in naphthoate ligands lowers the triplet state energy to such an extent that only europium luminescence is sensitised. Further conjugated systems (9-ACA) have triplet energies so low they are unsuitable to populate the $^5D_0$ state of europium. Although efforts to determine the triplet state energies of the gadolinium 9-ACA complexes failed, published results report values of around 14,400 cm^{-1}, which is in agreement with the observations made as part of this study [49].

Analysing the emission properties of the alkyl-substituted complexes, the triplet states are also of evident importance. Although triplet state energies are much higher than the terbium $^5D_4$ resonance level, efficient Tb^{3+} luminescence is observed for all complexes. The light output here seems mainly to be dominated by dynamic quenching such as energy transfer from the $^5D_4$ state to OH or CH oscillations (multiphonon relaxation) or terbium–terbium energy migration (self- or concentration quenching). In the case of the europium complexes, efficient light emission is observed for complexes whose triplet state energy is about 3000 cm^{-1} higher than the excited Eu^{3+} resonance levels. It appears that the emission intensity is higher for low energetic resonance levels such as $^5D_2$ (*p*-^{tert}BuBA, *m*-MeBA) compared with population of the higher energetic $^5D_3$ state (*o*-MeBA). This suggests that energy

Table 5
Absorption and emission properties of Eu and Tb carboxylate complexes.

Composition	Singlet–Singlet absorption		Emission integral (excitation efficiency)	
	Eu	Tb	Eu	Tb
$Ln(BA)_3(H_2O)_4$	N/A	250–290	N/A	$\lambda_{ex=295\,nm}$: 12 695 136 (15)^L
$Ln(BA)_3(H_2O)$	250–290	N/A	$\lambda_{ex=295\,nm}$: 1 913 362 (353)^L $\lambda_{ex=326\,nm}$: 543 245 (566)^D	N/A
$Ln(1\text{-}NA)_3(H_2O)$	250–340	250–350	$\lambda_{ex=341\,nm}$: 128 915 (353)^L $\lambda_{ex=366\,nm}$: 72 033 (10)^D	No luminescence observed
$Ln(2\text{-}NA)_3(H_2O)_2$	250–350	250–350	$\lambda_{ex=330\,nm}$: 1 106 247 (118)^L $\lambda_{ex=358\,nm}$: 914 506 (119)^D	No luminescence observed
$Ln(o\text{-}PhBA)_3(H_2O)_2$	250–315	250–305	$\lambda_{ex=302\,nm}$: 581 769 (35)^L $\lambda_{ex=370\,nm}$: 284 598 (69)^D	$\lambda_{ex=292\,nm}$: 2 675 599 (15)^L $\lambda_{ex=336\,nm}$: 1 925 256 (16)^D
$Ln(p\text{-}PhBA)_3(H_2O)_2$	250–350 345–370	250–310 335–365	$\lambda_{ex=304\,nm}$: 967 403 (88)^L $\lambda_{ex=356\,nm}$: 464 015 (95)^D	$\lambda_{ex=301\,nm}$: 1 005 856 (24)^L $\lambda_{ex=367\,nm}$: 722 348 (69)^D
$Ln(CA)_3$	250–325	250–330	$\lambda_{ex=290\,nm}$: 5 498 175 (74)^L $\lambda_{ex=337\,nm}$: 7 516 874 (80)^D $\lambda_{ex=358\,nm}$: 5 694 772 (87)^D	No luminescence observed
$Ln(9\text{-}ACA)_3$	250–400	250–400	No luminescence observed	No luminescence observed
$Ln(p\text{-}^{tert}BuBA)_3$	250–290	260–295	$\lambda_{ex=290\,nm}$: 3 874 181 (46)^L $\lambda_{ex=356\,nm}$: 1 621 454 (68)^D	$\lambda_{ex=285\,nm}$: 17 857 019 (17)^L
$Ln(o\text{-}MeBA)_3(H_2O)$	255–295	250–300	$\lambda_{ex=290\,nm}$: 1 071 810 (189)^L $\lambda_{ex=332\,nm}$: 476 844 (252)^D	$\lambda_{ex=296\,nm}$: 21 743 733 (21)^D $\lambda_{ex=360\,nm}$: 2 351 323 (24)^L
$Ln(m\text{-}MeBA)_3$	250–300	250–305	$\lambda_{ex=285\,nm}$: 2 788 453 (21)^L $\lambda_{ex=335\,nm}$: 1 392 716 (24)^D	$\lambda_{ex=301\,nm}$: 26 426 359 (19)^L $\lambda_{ex=351\,nm}$: 1 702 336 (29)^D
$Ln(p\text{-}MeBA)_3$	270–310	265–290	$\lambda_{ex=290\,nm}$: 754 231 (61)^L $\lambda_{ex=378\,nm}$: 511 187 (128)^D	$\lambda_{ex=286\,nm}$: 19 511 872 (19)^L $\lambda_{ex=323\,nm}$: 5 437 574 (19)^D
$Ln_2(Phth)_3(H_2O)_2$	250–300	250–295	$\lambda_{ex=294\,nm}$: 2 149 606 (53)^L $\lambda_{ex=370\,nm}$: 382 590 (59)^D	$\lambda_{ex=295\,nm}$: 15 279 186 (16)^L $\lambda_{ex=310\,nm}$: 10 119 210 (17)^D
$Ln_2(IsoPhth)_3(H_2O)_2$	250–295	250–300	$\lambda_{ex=295\,nm}$: 1 671 944 (41)^L $\lambda_{ex=370\,nm}$: 268 787 (38)^D	$\lambda_{ex=300\,nm}$: 12 550 737 (11)^L $\lambda_{ex=348\,nm}$: 3 447 064 (12)^D
$Ln_2(TerePhth)_3(H_2O)_4$	250–325	250–330	$\lambda_{ex=290\,nm}$: 1 713 028 (128)^L $\lambda_{ex=337\,nm}$: 1 284 387 (119)^D	$\lambda_{ex=296\,nm}$: 17 392 827 (14)^L $\lambda_{ex=330\,nm}$: 16 399 420 (14)^D

$^{L)}$ ligand excitation; $^{D)}$ direct excitation (*f*–*f* adsorption).

Table 6
Triplet state energies determined from room temperature phosphorescence measurements of the corresponding Gd^{3+} complexes.

Gd^{3+} complex	E_T in cm^{-1}	ΔE in cm^{-1}	
		Eu^{3+}	Tb^{3+}
BA	25,641*	8441 ($^5D_0$) 6591 ($^5D_1$) 4141 ($^5D_2$) 1241 ($^5D_3$) 641 ($^5L_6$)	5141 ($^5D_4$)
1-NA	19,084*	1884 ($^5D_0$) 34 ($^5D_1$)	<0
2-NA	19,231*	2031 ($^5D_0$) 181 ($^5D_1$)	<0
o-PhBA	23,095*	5895 ($^5D_0$) 4045 ($^5D_1$) 1595 ($^5D_2$)	2595 ($^5D_4$)
p-PhBA	20,492*	3292 ($^5D_0$) 1442 ($^5D_1$)	≈0
CA	20,408*	3208 ($^5D_0$) 1308 ($^5D_1$)	≈0
9-ACA	NA	NA	NA
p-$^{tert.}$BuBA	24,875*	7675 ($^5D_0$) 5825 ($^5D_1$) 3375 ($^5D_2$) 475 ($^5D_3$)	4372 ($^5D_4$)
o-MeBA	27,397*	10,197 ($^5D_0$) 8347 ($^5D_1$) 5897 ($^5D_2$) 2997 ($^5D_3$) 2397 ($^5L_6$)	6897 ($^5D_4$) 907 ($^5D_3$)
m-MeBA	25,316*	8116 ($^5D_0$) 6266 ($^5D_1$) 3816 ($^5D_2$) 916 ($^5D_3$) 316 ($^5L_6$)	8416 ($^5D_4$)
p-MeBA	24,630*	7430 ($^5D_0$) 5580 ($^5D_1$) 3130 ($^5D_2$) 230 ($^5D_3$)	4130 ($^5D_4$)
Phth	23,810	6610 ($^5D_0$) 4760 ($^5D_1$) 2310 ($^5D_2$)	3310 ($^5D_4$)
IsoPhth	23,923*	6723 ($^5D_0$) 4873 ($^5D_1$) 2423 ($^5D_2$)	3423 ($^5D_4$)
TerePhth	23,256*	6056 ($^5D_0$) 4206 ($^5D_1$) 1756 ($^5D_2$)	2759 ($^5D_4$)

* Measurements carried out at 110 K.

dissipates non-radiatively during internal conversion from higher excited europium $^5D_{1\text{-}4}$ levels to the $^5D_0$ emission levels. Although the energy difference is similar for the europium *p*-MeBA complex the light output is comparatively low. For quantum mechanical reasons (structural and electronic) the $^5D_0 \rightarrow {}^7F_J$ transition might be strongly forbidden, resulting in long living $^5D_0$ emission states, being sensitive to be involved in dynamic quenching. The fact that in the case of the terbium complexes the $^5D_4$ state is the resonance as well as the emission level, energy dissipating internal conversion processes are involved, resulting in large emission integrals compared with the europium luminescence. In this context it is also worth mentioning that in case of europium cinnamate an energy gap of 3000 cm^{-1} resulted in the highest emission integral determined for any europium complex included in this study. The same energy difference was assigned to be suitable to sensitise Eu^{3+} emission efficiently (above). Again, the reason for the remarkable emission intensity is the direct population of the $^5D_0$ emission level, rather than being populated from a higher ^5D resonance level as a result of internal conversion.

The triplet states of the dicarboxylic acids do not vary largely from each other (23,000 cm^{-1}) and consequently the light outputs are also similar. However, smaller energy differences seem to result in better luminescence (Eu-Phth: 2310 cm^{-1} to $^5D_2$; Tb-TerePhth: 2759 cm^{-1} for $^5D_4$).

2.7. Relaxation of selection rule due to J-mixing and crystal field coupling

All $^5D_0 \rightarrow {}^7F_J$ transitions are electric dipole forbidden due to quantum mechanical spin and parity selection rules. An exception, however, is the $^5D_0 \rightarrow {}^7F_1$ transition, which is magnetic dipole allowed ($\Delta J = 1$) and thus its intensity is independent to effects of the surrounding crystal field. Expressing the intensities of the forced electric dipole transitions relative to the absolute $^5D_0 \rightarrow {}^7F_1$ intensity provides an insight into the mechanism of the transition [12–17].

Analysing the $^5D_0 \rightarrow {}^7F_0$ transition, none of the states has a resulting total angular momentum quantum number J ($\Delta J = 0$), meaning that none of the states can interact with electromagnetic radiation, making this transition strictly forbidden. The only reason for the high intensity observed for the *o*-methylbenzoate complex (about 10 times higher) is coupling of different ^7F_J states (*J*-coupling), which usually only occurs in low symmetric complexes. Other complexes with a high $^5D_0 \rightarrow {}^7F_0$ intensity are europium *m*-methylbenzoate followed by *p*-^{tert}butylbenzoate.

While the $^5D_0 \rightarrow {}^7F_2$ transition is affected by both crystal field effects and *J*-mixing, the $^5D_0 \rightarrow {}^7F_4$ transition is only increased by crystal field mixing. Comparing the intensities of the emission lines of europium cinnamate, 1-naphthoate, *o*-phenylbenzoate, *p*-^{tert}butylbenzoate, *m*-methylbenzoate and isophthalate, the intensities of the $^5D_0 \rightarrow {}^7F_4$ transitions are weak (little crystal field mixing), while the $^5D_0 \rightarrow {}^7F_2$ transitions gained in intensity, meaning that the emission intensities are mainly governed by *J*-mixing rather than crystal field effects. Most distinct *J*-coupling is observed for the cinnamate, the *p*-^{tert}butylbenzoate and the *m*-methylbenzoate complex. It should also be mentioned that the *J*-mixing of the latter two complexes had already been suggested based on the relative intensities of the $^5D_0 \rightarrow {}^7F_0$ transitions.

The reverse situation (intensified $^5D_0 \rightarrow {}^7F_4$ transitions versus weakened $^5D_0 \rightarrow {}^7F_2$ transitions) can be observed for the europium benzoate, 2-naphthoate, *p*-phenylbenzoate and phthalate complexes. Since the low intensity of the $^5D_0 \rightarrow {}^7F_2$ transition suggests that the complexes are not affected by crystal field effects, the increase of the $^5D_0 \rightarrow {}^7F_4$ transition must be caused by vibronic distortion. Although this is thought to have only a minor effect on the overall intensity, the integrals of the low intensity $^5D_0 \rightarrow {}^7F_4$ transition might be affected to a larger extent than the integral of the $^5D_0 \rightarrow {}^7F_2$ transition. The intensity of the $^5D_0 \rightarrow {}^7F_4$ transition is highest for europium phthalate.

Finally, analysing the intensities of europium *o*-methylbenzoate, *p*-methylbenzoate and terephthalate, the $^5D_0 \rightarrow {}^7F_2$ transition as well as of the $^5D_0 \rightarrow {}^7F_4$ transition intensities are rather large, suggesting both crystal field mixing as well as *J*-coupling. This effect is rather distinctly observed in the case of *p*-methylbenzoate, which shows an extraordinarily high $^5D_0 \rightarrow {}^7F_2$ intensity.

2.8. Crystal field analysis

Having a *J* quantum number of zero, the $^5D_0$ emission level of Eu^{3+} is energetically non-degenerate, while the ^7F_J levels can split into 2J + 1 crystal field sub-levels, the splitting pattern governed

Table 7
Relative intensities and splitting pattern of the Eu^{3+} emission lines.

$^5D_0 \rightarrow {}^7F_J$ J=	Eu(BA)$_3$(H$_2$O)	Eu(1-NA)$_3$(H$_2$O)	Eu(2-NA)$_3$(H$_2$O)$_2$	Eu(CA)$_3$
0	0.033 (1)	0.029 (1)	0.033 (1)	0.027 (1)
1	1.000 (2)	1.000 (3)	1.000 (3)	1.000 (1)
2	3.188 (3)	5.345 (4)	3.188 (3)	7.518 (2)
3	0.003 (2)	0.113 (4)	0.063 (3)	0.119 (2)
4	0.409 (3)	0.300 (4)	0.409 (5)	0.287 (4)
$^5D_0 \rightarrow {}^7F_J$ J=	Eu(*o*-PhBA)$_3$(H$_2$O)$_2$	Eu(*p*-PhBA)$_3$(H$_2$O)$_2$	Eu(*p*-^{tert}BuBA)$_3$	Eu(*o*-MeBA)$_3$(H$_2$O)
0	0.034 (1)	0.031 (1)	0.051 (2)	0.229 (1)
1	1.000 (1)	1.000 (3)	1.000 (3)	1.000 (2)
2	4.484 (3)	3.179 (1)	6.383 (4)	4.508 (3)
3	0.078 (1)	0.065 (1)	0.615 (2)	0.147 (2)
4	0.291 (1)	0.389 (4)	0.314 (4)	0.402 (3)
$^5D_0 \rightarrow {}^7F_J$ J=	Eu(*m*-MeBA)$_3$	Eu(*p*-MeBA)$_3$	Eu$_2$(Phth)$_3$(H$_2$O)$_2$	Eu$_2$(IsoPhth)$_3$(H$_2$O)$_2$
0	0.116 (1)	0.036 (1)	0.028 (1)	0.034 (1)
1	1.000 (3)	1.000 (2)	1.000 (1)	1.000 (4)
2	4.980 (4)	6.684 (3)	3.550 (2)	4.006 (3)
3	0.141 (2)	0.133 (1)	0.115 (2)	0.129 (1)
4	0.284 (2)	0.447 (1)	0.441 (3)	0.266 (2)
$^5D_0 \rightarrow {}^7F_J$ J=				Eu$_2$(TerePhth)$_3$(H$_2$O)$_4$
0				0.031 (1)
1				1.000 (2)
2				4.360 (1)
3				0.124 (1)
4				0.400 (5)

by the crystal field and thus reflecting the micro-symmetry with regard to the europium centre. The presented results are based on Goerler-Walrand and Binnemans comprehensive review article, which correlates the crystal field-induced splitting patterns of the transition lines to coordination polyhedra based on the symmetry [19]. The number of observed components for the individual emission lines is listed in Table 7. The splitting patterns observed in the emission spectra were compared to the expected pattern based on the structure. Due to the low intensities of the low energetic transitions, only the $^5D_0 \rightarrow {}^7F_{0,1,2}$ transitions were used for crystal field analysis. However, it should be mentioned that the spectra were recorded at room temperature and accordingly the spectral resolution is low thus suggesting a lower symmetry. Additionally, perfect polyhedra are seldom formed, thus generating splitting patterns different from the theoretically expected ones. Due to these uncertainties it was decided not to relate the observed splitting patterns to any symmetry or coordination polyhedra.

The published structures of dysprosium benzoate and terbium terephthalate consist of square antiprismatic polyhedron with D_{4d} or D_4 symmetry. Based on these symmetries an approximate splitting pattern of 1:2:4 for the $^5D_0 \rightarrow {}^7F_{0,1,2}$ transitions is expected. While powder XRD and elemental analysis suggests that europium benzoate has a different structure and composition the Dy complex, a different splitting pattern is observed. Less lines than expected are present in the $^5D_0 \rightarrow {}^7F_2$ transition of the terephthalate complex, which is caused by the lack of spectral resolution of the room temperature measurements.

The splitting pattern of europium cinnamate matches the expected pattern of a trigonal symmetry (e.g., tricapped trigonal prism, D_{3h} or lower) of the isostructural lanthanum cinnamate complex except that the $^5D_0 \rightarrow {}^7F_1$ transition is short of one component caused by poor spectral resolution.

Although XRD results show that the synthesised europium *p*-methylbenzoate is not isostructural with the published single crystal structure the emission spectrum suggests a similar D_{3h} micro-symmetry (tricapped trigonal prism). Neodymium *m*-methylbenzoate forms the same polyhedron and is furthermore also isostructural to the corresponding Eu complex. However, an extra component is observed for the $^5D_0 \rightarrow {}^7F_1$ transition, which is caused by spectral noise.

The crystal structure of europium phthalate consists of two non-equivalent Eu centres, one being square antiprismatic (D_{4d} symmetry) and the other one being a distorted tricapped trigonal prism (D_{3h} symmetry). The large number of components produced by the two centres prevents a more detailed crystal field analysis. The $^5D_0 \rightarrow {}^7F_0$ emission of the europium *p*-^{tert}butylbenzoate complex consists of two components, indicating the presence of two different europium micro-environments. The complex splitting pattern observed of europium isophthalate also suggests the presence of more than one europium centres.

Being aware of the limitations, e.g., lack of spectral resolution of spectra recorded at room temperature as well as structural distortion, the splitting patterns of europium benzoate, *o*/*m*-methylbenzoate and *o*-phenylbenzoate suggest D_{3h} symmetry (trigonal prism, end-bicapped trigonal prism, pentacapped trigonal prism, anticuboctahedron and tricapped trigonal prism with the latter one being the most probable), while the naphthoates as well as *p*-phenylbenzoate seem to have C_{2v} symmetry (capped trigonal prism, bicapped octahedron and bicapped trigonal prism).

3. Conclusions

Various aromatic complexes of europium and terbium benzoates were synthesised following aqueous metathesis reactions. The compositions were determined by microanalysis, EDTA titrations and thermogravimetric analysis.

The structural phase was determined by powder XRD. It showed that most of the corresponding europium and terbium complexes were isomorphous, thus isostructural. Further structural conclusions were drawn from the IR spectra.

It has been shown that a crucial criterion affecting ligand sensitised lanthanoid emission is the energy of the triplet state. Observations suggest that the triplet state should be around 3000 cm^{-1} higher than the lanthanoid resonance level to result in efficient lanthanoid emission. While terbium emission is hardly affected by population of the high energetic $^5D_4$ resonance state (e.g., the resonance level is the emission level), higher energetic ^5D levels of europium are populated, followed by internal conversion do the $^5D_0$ emission state. Since internal conversion processes are accompanied by energy dissipation, the measured emission integrals are lower compared with terbium.

Conjugation lowers the triplet state energies to such an extent that at some stage only the low energy $^5D_0$ state of europium can be populated, and ligand sensitised terbium luminescence is not observed. Further conjugation lowers the triplet state to energies below the excited $^5D_0$ emission level, not being able to sensitise Eu^{3+} emission.

The triplet state energies of the alkyl-substituted carboxylates and dicarboxylates are suitable to populate the emission level ($^5D_4$) of terbium directly while higher energetic excited $^5D_{1\text{-}4}$ levels of europium are populated, resulting in a comparatively low light output.

An additional carboxylic acid substituent also results in efficiently populated ^5D states for europium and terbium. Additionally the excited lanthanoid states do not seem to be affected to a large extent by static quenching mechanisms. The light output of the dicarboxylate complexes seems to be determined by multiphonon relaxation and Ln–Ln energy transfer rather than inefficient population of the Ln resonance levels.

The substitution by alkyl groups, such as methyl and *tert*-butyl groups, lead to triplet state energies which are very efficiently populating the excited states of europium and terbium. The emission seems very insensitive towards static quenching mechanisms which can be concluded from the high emission integrals.

The splitting patterns of the Eu^{3+} emission, caused by crystal field interactions of the *J* level of the ^7F_J state, have been interpreted. The derived micro-symmetry matches that derived from published single crystal structures reasonably well. These structure are also in agreement with the observed separation of the $\nu_{as}(CO_2^-)$ and $\nu_s(CO_2^-)$ vibrations derived from infrared data.

The intensities of the $^5D_0 \rightarrow {}^7F_J$ transitions relative to the $^5D_0 \rightarrow {}^7F_1$ transition have been used to determine the electronic mechanism, such as *J*-coupling, ligand field mixing and vibrational distortion. These mechanisms add electric allowed character to the emissions, thus relaxing the strictness of the quantum mechanical selection rules.

4. Experimental

4.1. General procedures

The europium and terbium contents were determined by complexiometric EDTA titrations. Carbon contents were determined by a Carbon Sulfur Determinator ELTRA CS800. The combustion was carried out in the presence of tungsten and iron and the reaction took place in an oxygen stream. The instrument was calibrated using $BaCO_3$. The IR spectra were recorded in the range of 4000–650 cm^{-1} using a PerkinElmer Spektrum ATR spectrometer. DTA measurements were carried out in air, using a Netzsch STA 409 instrument, using aluminium oxide as a reference. The heat rate was 20 °C per minute and the weight and heat changes were determined in the range of 20–1000 °C. For phase analysis on the microcrystalline powders a Philips PW1130 equipped with a copper cathode ray tube PW2213/20 (60 kV, 1500 W) which generated Cu Kα radiation was used. A 2θ range of 5–50° was scanned. If available the recorded diffractograms were compared with those calculated from published single crystal structures computed on the data contained in the CCDC database using the program Lazy Pulverex. Photophysical properties of the complexes were determined using an ARC photospectrometer, which was equipped with a xenon discharge lamp (excitation source) and a photomultiplier (detection unit). The excitation and emission monochromators could be operated synchronised (reflectance spectra) or independently from each other (excitation and emission spectra). The powdered samples were thus irradiated with monochromatic light ranging from 250 to 400 nm for the acquisition of excitation and reflectance spectra.

The reflectance and thereby absorption $(1 - R)$ measurements were performed using a praying mantis set-up at an angle of incidence of ca. 50° to allow for a horizontal sample position. The powder samples were of a thickness of at least 1 mm. At this layer thickness, transmission through the sample is negligible due to diffuse back reflection, even for non-absorbing powders. Furthermore, the irradiated area is the same, both for powder and reference, thus, for relative measurements versus a known standard, further absorption correction is not required. The same holds true for the excitation and emission spectra, as described below.

The reflectance was detected by the photomultiplier, which was set to a sensitivity of 250 mV. No filters were used and the slit widths of both monochromators were set to 2 μm. Low wavelength sensitive gratings were used. Data were recorded in 1 nm intervals at three readings per point. The integration time was 500 ms.To eliminate wavelength dependent fluctuations in the lamp intensity and photomultiplier sensitivity as well as instrumental set-up parameters, a white standard (CaF_2), was measured under the same conditions. The sample data was divided by the data of the white standard in order to obtain the real reflectance spectrum of the sample. The emission monochromator was set to the characteristic emission wavelength of the individual lanthanoid ion (612 nm for Eu^{3+}, 545 nm for Tb^{3+}) whereas the excitation monochromator excited the sample with monochromatic light in the range of 250–400 nm. A long wavelength sensitive grating was used for the emission monochromator set to a slit width of 0.25 μm and equipped with a 350 nm cut-off filter, whereas for the excitation monochromator, set to a slit width of 2 μm and equipped with a UG5 filter, a short wavelength sensitive grating was used. Using a photomultiplier sensitivity of 600 mV data points were recorded in 1 nm intervals doing three readings per point and using an integration time of 500 ms. The excitation monochromator scanned the wavelength region between 250 and 400 nm. The excitation intensities were corrected by the multiplication of the wavelength dependent correction factor *k*. This was determined by characterising the standard phosphor BAM ($BaMgAl_{10}O_{17}:Eu^{2+}$) under the same conditions using the emission wavelength of 450 nm. Since the measured spectrum differs from the real BAM spectrum by a correction factor, this wavelength dependent factor *k* can be determined by dividing the intensities of the real BAM spectrum by the one measured with the instrument. The latter were provided by the Philips research laboratories in Aachen (Germany).

To characterise the emission properties of the complexes the instrument parameters regarding the filters, grating and slit widths were the same used to record the excitation spectra. However, the excitation monochromator was set to the wavelength of maximum excitation intensity, obtained from the excitation spectrum. The emission monochromator scanned the region between 400 and 700 nm in 0.25 nm steps doing three points per reading. Additionally the photomultiplier sensitivity was set to 1000 ms. To quantify the light output the emission intensities were integrated over the visible region. In order to eliminate influences resulting from the intensity of the xenon discharge excitation lamp, the emission integral was multiplied by the correction factor *k*, which was dependent on the excitation wavelength and which has been deter-

mined before from the excitation spectrum. To obtain information about the photophysical pathway, the integrals were also divided by the intensity of the excitation at the particular excitation wavelength, which was also obtained from the excitation spectrum. In the case of the europium complexes the intensities of the $^5D_0 \rightarrow {}^7F_0$ (578–582 nm), $^5D_0 \rightarrow {}^7F_2$ (605–635 nm), $^5D_0 \rightarrow {}^7F_3$ (640–665 nm) and $^5D_0 \rightarrow {}^7F_4$ (675–705 nm) transitions were integrated separately and the integral was given relative to the intensity of the magnetic allowed $^5D_0 \rightarrow {}^7F_1$ (582–605 nm) transition in order to draw conclusions about crystal field and *J*-mixing effects. Triplet emission spectra were measured with an Edinburgh Instruments FL 920 spectrometer equipped with a 450 W Xe source and a Hamamatsu extended red sensitivity photomultiplier tube. Samples were cooled to 110 K during the measurement with a Oxford Cryosystem device. Triplet positions were determined as the high-energy onset of the phosphorescence spectra.

4.2. General synthetic procedure

Europium chloride solutions were made by dissolving Eu_2O_3 in hot hydrochloric acid until it completely dissolved and then diluted with distilled water aiming on a final concentration of about 0.5 mol/dm^3. To obtain a terbium chloride solution, Tb_4O_7 was dissolved in concentrated nitric acid. Adding an excess of sodium carbonate solution, terbium carbonate precipitated and was washed with water until the filtrate showed a neutral pH. Terbium carbonate was then dissolved in hydrochloric acid and then continued as described for the europium solution. Both solutions were standardised by EDTA titrations (c_{EDTA} = 0.01 mol/dm^3), which in turn was standardised using a Zn^{2+} standard solution.

About 0.5 g of carboxylic acid ligand was suspended in water and Sodium carbonate solution was added until a pH of around five was reached and all insoluble acid was quantitatively converted into the soluble sodium salt. To this, the europium or terbium chloride solution was added aiming on a molar ratio lanthanoid:ligand of 1:3 (2:3 for the dicarboxylate ligands). An insoluble precipitate of the corresponding lanthanoid carboxylate complex was formed. The pH was again adjusted to five and the reaction mixtures were stirred over night to ensure completeness of the reaction. The suspensions were filtered and washed with ethanol and water. The product were then dried at room temperature to constant mass and then subjected to further investigations.

4.3. Physical data for all complexes

Stated here is mainly the synthetic data. Extracted information regarding the composition, DTA/DTG, IR and optical properties are presented in tables and the complete data can be found in the supplementary section. The IR data for all Gd complexes are only included in the supplementary material and was used to confirm structural similarity between Eu, Gd and Tb complexes.

$Eu(BA)_3(H_2O)$
V_{Eu}: 2.68 cm^3 (0.52 mol/dm^3) = 1.38 mmol
m_{HBA}: 0.51 g = 4.12 mmol
$m_{product}$: 0.40 g (yield = 54.5%)
$Tb(BA)_3(H_2O)_4$
V_{Tb}: 2.29 cm^3 (0.58 mol/dm^3) = 1.33 mmol
m_{HBA}: 0.49 g = 3.99 mmol
$m_{product}$: 0.62 g (yield = 78.6%)
$Eu(1\text{-}NA)_3(H_2O)$
V_{Eu}: 1.90 cm^3 (0.52 mol/dm^3) = 0.99 mmol
m_{H1NA}: 0.51 g = 2.97 mmol
$m_{product}$: 0.55 g (yield = 81.5%)
$Tb(1\text{-}NA)_3(H_2O)$
V_{Tb}: 1.69 cm^3 (0.58 mol/dm^3) = 0.98 mmol
m_{H1NA}: 0.51 g = 2.94 mmol
$m_{product}$: 0.55 g (yield = 81.4%)
$Eu(2\text{-}NA)_3(H_2O)_2$
V_{Eu}: 1.88 cm^3 (0.52 mol/dm^3) = 0.98 mmol
m_{H2NA}: 0.51 g = 2.94 mmol
$m_{product}$: 0.65 g (yield = 94.5%)
$Tb(2\text{-}NA)_3(H_2O)_2$
V_{Tb}: 1.98 cm^3 (0.58 mol/dm^3) = 1.15 mmol
m_{H2NA}: 0.59 g = 3.45 mmol
$m_{product}$: 0.75 g (yield = 91.8%)
$Eu(9\text{-}ACA)_3$
V_{Eu}: 1.52 cm^3 (0.52 mol/dm^3) = 0.79 mmol
m_{H9ACA}: 0.53 g = 2.37 mmol
$m_{product}$: 0.45 g (yield = 69.3%)
$Tb(9\text{-}ACA)_3$
V_{Tb}: 1.36 cm^3 (0.58 mol/dm^3) = 0.79 mmol
m_{H9ACA}: 0.52 g = 2.37 mmol
$m_{product}$: 0.40 g (yield = 36.2%)
$Eu(CA)_3$
V_{Eu}: 2.42 cm^3 (0.52 mol/dm^3) = 1.26 mmol
m_{HCA}: 0.56 g = 3.78 mmol
$m_{product}$: 0.71 g (yield = 94.7%)
$Tb(CA)_3$
V_{Tb}: 2.05 cm^3 (0.58 mol/dm^3) = 1.19 mmol
m_{HCA}: 0.53 g = 3.57 mmol
$m_{product}$: 0.67 g (yield = 93.2%)
$Eu(o\text{-}PhBA)_3(H_2O)_2$
V_{Eu}: 1.77 cm^3 (0.52 mol/dm^3) = 0.92 mmol
$m_{H\text{-}o\text{-}PhBA}$: 0.55 g = 2.76 mmol
$m_{product}$: 0.52 g (yield = 73.0%)
$Tb(o\text{-}PhBA)_3(H_2O)_2$
V_{Tb}: 1.57 cm^3 (0.58 mol/dm^3) = 0.91 mmol
$m_{H\text{-}o\text{-}PhBA}$: 0.54 g = 2.73 mmol
$m_{product}$: 0.32 g (yield = 45.0%)
$Eu(p\text{-}PhBA)_3(H_2O)_2$
V_{Eu}: 1.83 cm^3 (0.52 mol/dm^3) = 0.95 mmol
$m_{H\text{-}p\text{-}PhBA}$: 0.56 g = 2.85 mmol
$m_{product}$: 0.63 g (yield = 84.9%)
$Tb(p\text{-}PhBA)_3(H_2O)_2$
V_{Tb}: 1.53 cm^3 (0.58 mol/dm^3) = 0.89 mmol
$m_{H\text{-}p\text{-}PhBA}$: 0.53 g = 2.67 mmol
$m_{product}$: 0.62 g (yield = 88.1%)
$Eu(p\text{-}tert.BuBA)_3$
V_{Eu}: 1.00 cm^3 (0.52 mol/dm^3) = 1.04 mmol
$m_{Hp\text{-}tert.BuBA}$: 0.55 g = 3.06 mmol
$m_{product}$: 0.56 g (yield = 77.4%)
$Tb(p\text{-}tert.BuBA)_3$
V_{Tb}: 1.72 cm^3 (0.58 mol/dm^3) = 1.00 mmol
$m_{Hp\text{-}tert.BuBA}$: 0.45 g = 3.00 mmol
$m_{product}$: 0.g (yield = 65.2%)
$Eu(o\text{-}MeBA)_3(H_2O)$
V_{Eu}: 2.50 cm^3 (0.52 mol/dm^3) = 1.30 mmol
$m_{H\text{-}o\text{-}MeBA}$: 0.53 g = 3.90 mmol
$m_{product}$: 0.58 g (yield = 78.9%)
$Tb(o\text{-}MeBA)_3(H_2O)$
V_{Tb}: 2.34 cm^3 (0.58 mol/dm^3) = 1.36 mmol
$m_{H\text{-}o\text{-}MeBA}$: 0.56 g = 4.08 mmol
$m_{product}$: 0.51 g (yield = 64.9%)
$Eu(m\text{-}MeBA)_3$
V_{Eu}: 2.52 cm^3 (0.52 mol/dm^3) = 1.31 mmol
$m_{H\text{-}m\text{-}MeBA}$: 0.53 g = 3.93 mmol
$m_{product}$: 0.46 g (yield = 63.4%)
$Tb(m\text{-}MeBA)_3$
V_{Tb}: 2.24 cm^3 (0.58 mol/dm^3) = 1.30 mmol

$m_{\text{H-}m\text{-MeBA}}$: 0.53 g = 3.90 mmol
m_{product}: 0.40 g (yield = 54.5%)

$Eu(p\text{-MeBA})_3$
V_{Eu}: 2.75 cm^3 (0.52 mol/dm^3) = 1.43 mmol
$m_{\text{H-}p\text{-MeBA}}$: 0.58 g = 4.29 mmol
m_{product}: 0.53 g (yield = 66.9%)

$Tb(p\text{-MeBA})_3$
V_{Tb}: 2.52 cm^3 (0.58 mol/dm^3) = 1.46 mmol
$m_{\text{H-}p\text{-MeBA}}$: 0.60 g = 4.38 mmol
m_{product}: 0.66 g (yield = 79.7%)

$Eu_2(Phth)_3(H_2O)_2$
V_{Eu}: 4.09 cm^3 (0.52 mol/dm^3) = 2.13 mmol
$m_{\text{HH-Phth}}$: 0.53 g = 3.19 mmol
m_{product}: 0.48 g (yield = 53.1%)

$Tb_2(Phth)_3(H_2O)_2$
V_{Tb}: 3.60 cm^3 (0.58 mol/dm^3) = 2.09 mmol
$m_{\text{HH-Phth}}$: 0.52 g = 3.13 mmol
m_{product}: 0.89 g (yield = 98.7%)

$Eu_2(IsoPhth)_3(H_2O)_2$
V_{Eu}: 3.94 cm^3 (0.52 mol/dm^3) = 2.05 mmol
$m_{\text{HH-IsoPhth}}$: 0.51 g = 3.07 mmol
m_{product}: 0.77 g (yield = 90.3%)

$Tb_2(IsoPhth)_3(H_2O)_2$
V_{Tb}: 3.60 cm^3 (0.58 mol/dm^3) = 2.09 mmol
$m_{\text{HH-IsoPhth}}$: 0.52 g = 3.13 mmol
m_{product}: 0.71 g (yield = 80.49%)

$Eu_2(TerePhth)_3(H_2O)_4$
V_{Eu}: 3.94 cm^3 (0.52 mol/dm^3) = 2.05 mmol
$m_{\text{HH-TerePhth}}$: 0.51 g = 3.07 mmol
m_{product}: 0.57 g (yield = 84.4%)

$Tb_2(TerePhth)_3(H_2O)_4$
V_{Tb}: 3.67 cm^3 (0.58 mol/dm^3) = 2.13 mmol
$m_{\text{HH-TerePhth}}$: 0.53 g = 3.19 mmol
m_{product}: 0.85 g (yield = 88.9%)
Contents: Tb = 37.2% (calculated for $Tb_2C_{24}H_{20}O_{16}$: Tb = 36.0%)

Gd complexes
BA
V_{Gd}: 2.74 cm^3 (0.52 mol/dm^3) = 1.37 mmol
m_{HBA}: 0.50 g = 4.10 mmol
1-NA
V_{Gd}: 1.94 cm^3 (0.52 mol/dm^3) = 0.97 mmol
$m_{\text{H-1NA}}$: 0.50 g = 2.90 mmol
2-NA
V_{Gd}: 1.94 cm^3 (0.52 mol/dm^3) = 0.97 mmol
$m_{\text{H-2NA}}$: 0.50 g = 2.90 mmol
9-ACA
V_{Gd}: 1.50 cm^3 (0.52 mol/dm^3) = 0.75 mmol
$m_{\text{H-9ACA}}$: 0.50 g = 2.25 mmol
CA
V_{Gd}: 2.25 cm^3 (0.52 mol/dm^3) = 1.13 mmol
m_{HCA}: 0.50 g = 3.37 mmol
o-PhBA
V_{Gd}: 1.61 cm^3 (0.52 mol/dm^3) = 0.84 mmol
$m_{\text{H-}o\text{PhBA}}$: 0.50 g = 2.52 mmol
p-PhBA
V_{Gd}: 1.61 cm^3 (0.52 mol/dm^3) = 0.84 mmol
$m_{\text{H-}p\text{PhBA}}$: 0.50 g = 2.52 mmol
p-^{tert}BuBA
V_{Gd}: 1.80 cm^3 (0.52 mol/dm^3) = 0.94 mmol
$m_{\text{H-}p\text{tertBuBa}}$: 0.50 g = 2.80 mmol
o-MeBA
V_{Gd}: 2.35 cm^3 (0.52 mol/dm^3) = 1.22 mmol
$m_{\text{H-}o\text{MeBA}}$: 0.50 g = 3.67 mmol
m-MeBA
V_{Gd}: 2.35 cm^3 (0.52 mol/dm^3) = 1.22 mmol
$m_{\text{H-}m\text{MeBA}}$: 0.50 g = 3.67 mmol
p-MeBA
V_{Gd}: 2.35 cm^3 (0.52 mol/dm^3) = 1.22 mmol
$m_{\text{H-}p\text{MeBA}}$: 0.50 g = 3.67 mmol
Phth
V_{Gd}: 3.85 cm^3 (0.52 mol/dm^3) = 2.00 mmol
$m_{\text{HH-Phth}}$: 0.50 g = 3.00 mmol
IsoPhth
V_{Gd}: 3.85 cm^3 (0.52 mol/dm^3) = 2.00 mmol
$m_{\text{HH-IsoPhth}}$: 0.50 g = 3.00 mmol
TerePhth
V_{Gd}: 3.85 cm^3 (0.52 mol/dm^3) = 2.00 mmol
$m_{\text{HH-TerePhth}}$: 0.50 g = 3.00 mmol

Acknowledgements

We acknowledge the Australian Research Council for support. We also acknowledge an IPRS scholarship and Monash Graduate Scholarship (M.H.).

Appendix A. Supplementary data

Supplementary data associated with this article can be found, in the online version, at doi:10.1016/j.jphotochem.2008.10.026.

References

[1] T. Steinkamp, F. Schweppe, B. Krebs, U. Karst, Analyst 128 (2003) 29–31.
[2] D. Kumar, K.G. Cho, Z. Chen, V. Craciun, P.H. Holloway, R.K. Singh, Phys. Rev. B 60 (1999) 13331–13334.
[3] J.M. De Souza, S. Alves, G.F. De Sa, W.M. De Azevedo, J. Alloys Compd. 344 (2002) 320–322.
[4] Z.Q. Gao, C.S. Lee, I. Bello, S.T. Lee, Synth. Met. 111–112 (2000) 39–42.
[5] M. Guan, Z.Q. Bian, F.Y. Li, H. Xin, C.H. Huang, New. J. Chem. 27 (2003) 1731–1734.
[6] S.H. Cho, S.H. Kwon, J.S. Yoo, C.W. Oh, J.D. Lee, K.J. Hong, S.J. Kwon, J. Electrochem. Soc. 147 (2000) 3143–3147.
[7] D. Parker, P.K. Senanayake, J.A.G. Williams, J. Chem. Soc. Perk. Trans. 2 (10) (1998) 2129–2139.
[8] Y. Fukuda, H. Ohtaki, A. Tomita, S. Owaki, Radiat. Prot. Dosim. 65 (1996) 325–328.
[9] A. Beeby, S.W. Botchway, I.M. Clarkson, S. Faulkner, A.W. Parker, D. Parker, J.A.G. Williams, J. Photoch. Photobiol. B 57 (2000) 83–89.
[10] T. Justel, H. Bechtel, H. Nikol, C.R. Ronda, D.U. Wiechert, Proc. Electrochem. Soc. 98–24 (1999) 103–119.
[11] Y. Taguchi, H. Koda, K. Ogi, Photopolymer laminate and its use in signboard with long afterglow in dark (Patent Number 2002321316) Kokai Tokkyo Koho. 2002 (Toyobo Co., Ltd., Japan), 5.
[12] B.R. Judd, Atomic theory and optical spectroscopy, in: K.A. Gschneidner, L. Eyring (Eds.), Handbook on the Physics and Chemistry of the Rare Earths, North-Holland Publishing Company, 1988, p. 81.
[13] Z.B. Goldschmidt, Atomic properties (free atom atomic theory and optical spectroscopy, in: K.A. Gschneidner, L. Eyring (Eds.), Handbook on the Physics and Chemistry of the Rare Earths, North-Holland Publishing Company, 1978, p. 1.
[14] P. Fulde, Crystal fields, atomic theory and optical spectroscopy, in: K.A. Gschneidner, L. Eyring (Eds.), Handbook on the Physics and Chemistry of the Rare Earths, North-Holland Publishing Company, 1979, p. 295.
[15] W.T. Carnall, The absorption and emission spectra of rare earth ions in solution, atomic theory and optical spectroscopy, in: K.A. Gschneidner, L. Eyring (Eds.), Handbook on the Physics and Chemistry of the Rare Earths, North-Holland Publishing Company, 1979, p. 171.
[16] C.A. Morrison, R.P. Leavitt, Spectroscopic properties of triplyionised lanthanides in transparent host crystals, atomic theory and optical spectroscopy, in: K.A. Gschneidner, L. Eyring (Eds.), Handbook on the Physics and Chemistry of the Rare Earths, North-Holland Publishing Company, 1982, p. 461.
[17] M. Dolg, H. Stoll, Electronic structure calculations for molecules containing lanthanoid atoms, atomic theory and optical spectroscopy, in: K.A. Gschneidner, L. Eyring (Eds.), Handbook on the Physics and Chemistry of the Rare Earths, Elsevier, 1996, p. 607.
[18] D. Garcia, M. Faucher, Crystal field in non-metallic (rare earth) compounds, atomic theory and optical spectroscopy, in: K.A. Gschneidner, L. Eyring (Eds.), Handbook on the Physics and Chemistry of the Rare Earths, Elsevier, 1995, p. 263.
[19] C. Görller-Walrand, K. Binnemans, Rationalization of crystal field parameterization, atomic theory and optical spectroscopy, in: K.A. Gschneidner, L. Eyring (Eds.), Handbook on the Physics and Chemistry of the Rare Earths, Elsevier, 1996, p. 121.

[20] D.F. Shriver, P.W. Atkins, C.H. Langford, Anorganische Chemie, first ed., VCH, Weinheim, 1992.
[21] F.A. Cotton, G. Wilkinson, Advanced Inorganic Chemistry, vol. 4, fourth ed., Wiley & Sons, 1980.
[22] D. Parker, Coord. Chem. Rev. 205 (2000) 109–130.
[23] S. Shionoya, W.M. Yen, Phosphor Handbook, first ed., CRC Press, 1997.
[24] N. Sabbatini, M. Guardigli, I. Manet, Antenna effect in encapsulation complexes of lanthanide ions, in: K.A. Gschneidner, L. Eyring (Eds.), Handbook on the Physics and Chemistry of the Rare Earths, Elsevier, 1996, p. 69.
[25] J.M. Lehn, Angew. Chem. Int. Ed. 29 (1990) 1304–1319.
[26] M.C.F.C. Felinto, C.S. Tomiyama, H.F. Brito, E.E.S. Teotonio, O.L. Malta, J. Solid State Chem. 171 (2003) 189–194.
[27] J. Dexpert-Ghys, C. Picard, A. Taurines, J. Inclusion Phenom. 39 (2001) 261–267.
[28] A.W.-H. Lam, W.T. Wong, S. Gao, G. Wen, X.-X. Zhang, Eur. J. Inorg. Chem. (2003) 149–163.
[29] J.C.G. Buenzli, D. Wessner, Israel J. Chem. 24 (1984) 313–322.
[30] H. Bußkamp, G.B. Deacon, M. Hilder, P.C. Junk, U.H. Kynast, W.W. Lee, D.R. Turner, Cryst. Eng. Comm. 9 (2007) 394–411.
[31] L.D. Carlos, M. Assuncao, L. Alcacer, Synth. Met. 69 (1995) 587–588.
[32] M. Bredol, T. Justel, S. Gutzov, Opt. Mater. 18 (2001) 337–341.
[33] D. De Graaf, S.J. Stelwagen, H.T. Hintzen, G. De With, J. Non-Cryst. Solids 325 (2003) 29–33.
[34] H. Deng, D.L. Gin, 215th ACS National Meeting (Book of Abstracts), 1998, POLY-214.
[35] M. Bredol, U. Kynast, C. Ronda, T. Welker, Luminescent materials and methods for their preparation (Patent number 4122009) 1993 (Philips Patentverwaltung G.m.b.H., Germany), 3.
[36] D. Sendor, P. Junk, U. Kynast, Solid State Phenom. 90–91 (2003) 521–526.
[37] Z.-M. Wang, L.J. van de Burgt, G.R. Choppin, Inorg. Chim. Acta 293 (1999) 167–177.
[38] A. De Bettencourt-Dias, Inorg. Chem. 44 (2005) 2734–2741.
[39] R.C. Mehrotra, R. Bohra, Metal Carboxylates, first ed., Academic Press, 1983.
[40] G.B. Deacon, R.J. Phillips, Coord. Chem. Rev. 33 (1980) 227–250.
[41] M.S. Khiyalov, I.R. Amiraslanov, F.N. Musaev, K.S. Mamedov, Koord. Khim. 8 (1982) 548–552.
[42] Q.H. Jin, X. Li, Y.Q. Zou, K.B. Yu, Acta Crystallogr. Sect. C 57 (2001) 676–677.
[43] J. Ma, Z. Jin, J. Ni, Huaxue Xuebao 51 (1993) 265–272.
[44] Y. Wan, L. Jin, K. Wang, L. Zhang, X. Zheng, S. Lu, New. J. Chem. 26 (2002) 1590–1596.
[45] T.M. Reineke, M. Eddaoudi, M. Fehr, D. Kelley, O.M. Yaghi, J. Am. Chem. Soc. 121 (1999) 1651–1657.
[46] W.-M. Lu, W.-G. Chen, X.-Y. Luo, N. Dong, K.-L. Liang, Y.-Q. Huang, S.-Z. Hu, Gaodeng Xuexiao Huaxue Xuebao 18 (1997) 337–341.
[47] G. Blasse, B.C. Grabmaier, Luminescent Materials, first ed., Springer Verlag, 1994.
[48] (a) J. Reshmi, S. Biju, M. Reddy, Inorg. Chem. Commun. 10 (2007) 1091–1094; (b) M. Latva, H. Takalo, V.M. Mukkala, C. Matachescu, J.C. RodriguezUbis, J. Kankare, J. Luminescence 75 (1997) 149–169.
[49] L. Ruan, H. Wang, Y. Hao, H. Zhou, X. Liu, B. Xu, J. Luminescence 122–123 (2007) 467–470.